Journal of Ocean Engineering and Marine Energy (2019) 5:85–98
https://doi.org/10.1007/s40722-019-00132-z

RESEARCH ARTICLE

A note on the tuning of tidal turbines in channels

Lei Chen[1] · Paul A. J. Bonar[2] · Christopher R. Vogel[1] · Thomas A. A. Adcock[1]

Received: 17 December 2018 / Accepted: 27 February 2019 / Published online: 11 March 2019

Abstract
Maximising the performance of a tidal turbine array requires the turbine resistance to be 'tuned' for a given channel and turbine arrangement. In many cases, tuning the turbines to produce the maximum power coefficient presents too great a resistance to the incoming flow and results in a lower power output. Recent studies have shown that, as compared to using a fixed tuning, considerably more power can be produced by varying the turbine resistance over the tidal cycle. To our knowledge, however, this higher power output has only been demonstrated for highly idealised models, which use an additional drag force or a uniformly porous disc to represent the turbines. In this study, we re-examine these tuning strategies using a more realistic turbine model, which is based on the blockage-corrected blade element momentum theory. We find that, as compared to the idealised actuator disc, the importance of tuning is significantly reduced for the more realistic tidal rotor, and that this is particularly true for rotors with fixed blade pitch. We also find that the maximum amount of power produced by the blade element momentum rotor, averaged over the tidal cycle, is typically 60–70% of that produced by the actuator disc.

Keywords Tidal stream power · Tidal turbine · Tidal channel · Actuator disc theory · Blade element momentum theory

1 Introduction

Much of the global tidal stream power resource is located in narrow channels, where the energy present in the tidal flow is concentrated to produce fast tidal streams (Vennell et al. 2015). In extracting part of this energy, however, tidal turbines present an additional resistance to flow, which acts to slow and divert these streams. Understanding this interaction between the turbines and the incoming flow is vital to the accurate assessment of tidal stream power resources and the optimal design of tidal turbine arrays (Adcock et al. 2015).

Vennell (2010) was the first to show that maximising the performance of a tidal turbine array requires the turbine resistance to be 'tuned' for a given channel and turbine arrangement. By combining the simple tidal channel and bounded actuator disc models of Garrett and Cummins (2005, 2007), Vennell (2010) showed that for turbines in channels, the maximum power depends not only on the power coefficient, but also on the thrust coefficient, which, together with the channel's natural dynamic balance, determines the throughflow velocity. Vennell (2010) also showed that large, optimally tuned turbine arrays can realise most of a channel's energy potential, and later demonstrated, following Adcock (2012), that varying the tuning over the tidal cycle can produce a higher power output, often without increasing the maximum loading on the turbines and whilst also maintaining a higher channel flow rate (Vennell 2016).

The works of Vennell (2010, 2016) provide key insights into the importance of tuning for tidal turbines in channels, but are, to a certain extent, limited by their turbine representation. Actuator disc theory provides a useful starting point for the analysis of tidal turbine performance, and has proven valuable in establishing upper bounds on the power available to rows of turbines placed at candidate tidal power sites (e.g. Adcock et al. 2013). However, modelling the turbine rotor as a uniformly porous disc neglects the structure of the turbine blades, and thus offers only an idealised description of turbine performance (e.g. Hau and von Renouard 2003; Burton et al. 2001).

In this paper, the works of Vennell (2010, 2016) are extended to incorporate a more realistic turbine representation, which is based on the blockage-corrected blade element momentum theory of Vogel et al. (2018). This more advanced low-order model relates the flow through the turbine plane to

✉ Thomas A. A. Adcock
thomas.adcock@eng.ox.ac.uk

[1] Department of Engineering Science, University of Oxford, Parks Road, Oxford OX1 3PJ, UK

[2] School of Engineering, University of Edinburgh, Mayfield Road, Edinburgh EH9 3FB, UK

the blade forces developed by the rotor, and may be used to consider different approaches to turbine tuning, which include varying the rotational speed and/or pitch angle of the turbine blades. As well as providing a broader parameter space within which to explore turbine performance, the introduction of the tidal rotor affords opportunities to re-examine the importance of tuning for tidal turbines in channels and to compare the actuator disc, which has been used extensively in theoretical and numerical models of tidal stream power, with a more realistic model of turbine performance.

This study presents the blockage-corrected blade element momentum rotor as a potential replacement for the actuator disc. Though blade element momentum theory retains a number of simplifying assumptions, it offers a more accurate description of turbine performance than does the porous disc, and at only marginally greater computational cost. For the blade element model, the performance also depends, naturally, on the design of the rotor. Given that the blades selected are broadly representative of those which may be used for tidal power, however, this analysis should provide useful, general insights into the importance of tuning for tidal turbines, and its role in maximising the power available from tidal channels.

2 Model

2.1 Tidal channel

A simple analytical model, which has been used extensively in the theoretical study of tidal stream power (e.g. Garrett and Cummins 2005; Vennell 2010; Adcock and Draper 2014), is used to describe head-driven flow through an idealised tidal channel connecting two infinite oceans. Though simplistic, this model is able to capture the leading-order effects of energy extraction on channel dynamics at low computational cost, which simplifies greatly the process of optimising turbine deployments.

As in previous studies, a number of assumptions are made to simplify the analysis. First, it is assumed that the channel is sufficiently short that the volumetric flow rate does not vary along its length. It is then assumed that the variation in water depth within the channel is sufficiently small that the cross-sectional area of the flow does not vary in time. Assuming a single-constituent tide, a quadratic seabed drag, and negligible drag from turbine support structures, the equation governing the channel-scale flow may then be presented in dimensionless form, following Garrett and Cummins (2005), as

$$\frac{\mathrm{d}Q}{\mathrm{d}t} + (\lambda_1 + \lambda_0)Q|Q| = \cos(t), \tag{1}$$

and solved using a fourth-order Runge–Kutta method. The key dimensionless parameters are the volumetric flow rate, Q, turbine drag, λ_1, and natural dynamic balance, λ_0, which describes how the tidal forcing is balanced, in the absence of turbines, by the drag and inertial forces acting on the flow. Realistic values for the latter term typically range between $\lambda_0 = 0.1$ for deep, 'inertia-dominated' channels and $\lambda_0 = 5$ for shallow, 'drag-dominated' channels (Vennell et al. 2015), but a broad range of values is considered herein: $0 \leq \lambda_0 \leq 10$.

Garrett and Cummins (2005) have shown that there is a maximum amount of power that can be extracted from a tidal channel, and that both this maximum extractable power and the optimal turbine drag, λ_1, depend solely on the value of λ_0. A recent study by Kreitmair et al. (2019) has used this simple channel model to show how uncertainty in the value of specific inputs (the bed roughness coefficient, in this case) can propagate through the model to produce uncertain optimal tunings and maximum power estimates. Uncertainty will be an important consideration for studies of real tidal power sites, where bed roughness and other parameters must be carefully calibrated prior to undertaking resource assessments, but is not considered in this study, where the aim is simply to compare between different idealised models of turbine performance.

This study focuses on maximising the time average of the power available to the turbines after the subtraction of local-scale wake mixing losses (e.g. Adcock et al. 2013). This quantity may be expressed in dimensionless form, following Adcock and Draper (2014), as

$$P = \frac{1}{2}NBC_\mathrm{P}|Q^3|, \tag{2}$$

in which N is the (non-dimensional) number of (full-width) turbine rows, C_P is the turbine power coefficient, and B is the blockage, which is defined as the ratio of turbine swept area to flow cross-sectional area. If the turbine resistance is held constant throughout the tidal cycle, the task of maximising P is trivial: a fixed tuning is used to achieve a certain C_P and hence P, the value of which may be maximised by selecting the optimal fixed tuning. The task becomes quite complex, however, if the tuning parameters are allowed to vary in time.

To simplify this more complicated optimisation problem, the tidal cycle is divided into M equal sub-cycles. Within each of these shorter periods, the turbine resistance is held constant and a simple optimisation algorithm, which begins with a selection of pseudorandom variables, is used to determine the set of fixed tunings which maximise P. In this way, M fixed tunings over M sub-cycles are used to approximate the optimal temporally varying tuning. The optimal M fixed tunings are obtained herein using MATLAB's 'GlobalSearch' function, and the resulting value of P_max is found to be insensitive

to the initial set of pseudorandom variables. Model solutions do depend on the choice of M, but the resulting value of $P_{\max}$ is found to converge with increasing M. Increasing the value of M above 20 is found to yield increases in $P_{\max}$ of $< 1\%$, and so a value of $M = 20$ is chosen for ease of computation.

2.2 Actuator disc

Actuator disc theory provides perhaps the simplest description of an axial flow turbine. In the theory, the rotor, which comprises a number of blades rotating about a central hub, is described as a simple porous disc which presents a uniform resistance to the flow passing through it. The concept of the actuator disc is well established in the literature; a detailed account of the underlying theory is provided by Burton et al. (2001).

Having proven valuable in the analysis of wind turbines, actuator disc theory was adapted for use with tidal turbines by Garrett and Cummins (2007), who extended the classical unbounded theory due to Betz (1920) and Joukowsky (1920) to incorporate the effects of blockage. To achieve this, Garrett and Cummins (2007) replaced the unbounded flow field with a volume-flux-constrained flow field, which describes bounded flow with a 'rigid lid'; that is to say, a free surface which does not deform in response to energy extraction. The bounded disc model of Garrett and Cummins (2007) has since been further extended to explore more realistic flow conditions (e.g. Houlsby et al. 2008; Vennell 2010; Draper et al. 2013, 2016) and optimal arrangements for tidal turbines (e.g. Nishino and Willden 2012; Draper and Nishino 2014a, b; Vogel et al. 2016; Gupta and Young 2017).

The key parameters in this bounded disc model are the blockage, B, basin efficiency, η (which is defined, following Adcock et al. (2013), as the ratio of available power, P, to the total amount of power removed from the flow), and turbine tuning, which is represented herein by a local resistance coefficient, k, defined, following Draper et al. (2014), as

$$k = \frac{b_4^2 - (1 - a_4)^2}{(1 - a_2)^2}, \tag{3}$$

in which a_2 is the rotor induction factor, a_4 is the wake induction factor, and b_4 is the wake bypass velocity coefficient. In the case of volume-flux-constrained flow, Draper et al. (2014) showed that the maximum power coefficient is achieved by tuning the turbines such that

$$k = \frac{2(1 + B)^3}{(1 - B)^2}, \tag{4}$$

and so an optimal value of $k = 2$ is obtained for the classical unbounded flow analysis from which the well-known Betz limit is derived.

Actuator disc models have been widely used in theoretical and numerical studies of tidal stream power. However, the simple porous disc offers only an idealised description of turbine performance, and is expected to provide an overestimate of the power that would be available to an actual turbine. Moreover, the actuator disc model does not account for the structure of the turbine blades and so cannot be used to compare between different blade designs or different approaches to turbine tuning (e.g. Hau and von Renouard 2003).

2.3 Blade element momentum rotor

Blade element momentum theory combines linear momentum theory with blade element theory to offer a more advanced low-order turbine model which can account for the structure of the blades, and thus provide a more realistic description of turbine performance (Glauert 1983). A brief description of the theory will suffice here; the reader is again directed to Burton et al. (2001) for further detail.

In blade element theory, the n blades rotating at angular velocity ω are divided along their spanwise length R into Z blade elements, the swept areas of which take the form of Z concentric annular rings (Fig. 1a). The lift and drag forces on each element are calculated from two-dimensional aerofoil characteristics by specification of the axial induction factor, a_2, tangential induction factor, a_2', relative velocity, W, blade pitch angle, β, and attack angle, α (Fig. 1b).

Neglecting spanwise velocities and three-dimensional flow effects, the axial and tangential velocities for each blade element are given by $(1-a_2)U$ and $(1+a_2')\omega r$, respectively, in which U is the axial velocity and r is the spanwise distance from the blade root. The sectional lift force, δL, acting on a spanwise length, δr, of the blade and in a direction normal to that of W is then given, following Burton et al. (2001), as

$$\delta L = \frac{1}{2}\rho W^2 c C_{\mathrm{L}} \delta r, \tag{5}$$

in which ρ is the fluid density, c is the chord length of the blade section (marked by the dashed line in Fig. 1b), and C_{L} is the lift coefficient. The sectional drag force, δD, acting on the spanwise length δr and in the direction of W, is then given by

$$\delta D = \frac{1}{2}\rho W^2 c C_{\mathrm{D}} \delta r, \tag{6}$$

in which C_{D} is the drag coefficient.

In blade element momentum theory, the forces acting on each annular ring are related to the change in the momentum of the fluid passing through the rotor. Spanwise velocities are neglected, so it is assumed that there is no momentum transfer between annular elements. The theory also assumes that all

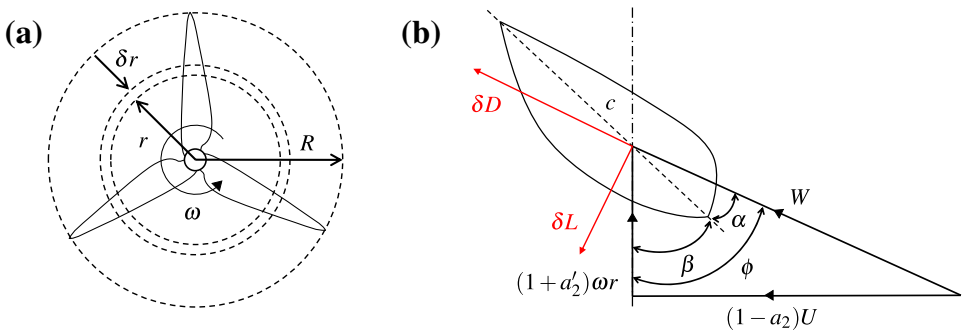

Fig. 1 Schematic diagrams showing: **a** the discretisation of the turbine rotor into annular rings, and; **b** the resolution of lift and drag forces on each blade section. Adapted from Burton et al. (2001) (colour online)

fluid particles passing through a given annular element experience the same change in momentum, which neglects the gaps between the blades (Burton et al. 2001). To account for this, a simple tip correction method is used: the blade thrust and torque are multiplied by a dimensionless tip correction factor, F, given by

$$F = \frac{2}{\pi}\cos^{-1}\left[\exp\left[\frac{n(1-(R/r))}{2\sin\phi}\right]\right], \tag{7}$$

in which $\phi = \alpha+\beta$ is the incident flow angle formed between W and the plane of blade rotation. With this function, F is assigned a value of unity for most of the blade span, where the gaps between the blades are assumed to be small, but decreases to zero near the blade tip, where the gaps are much larger (Eggleston and Stoddard 1987).

Blade element momentum theory also gives expressions for the sectional axial thrust, δT, and tangential torque, $\delta\tau$, acting on the spanwise length δr. These may be equated to the changes in axial and angular momentum, respectively, of the flow passing through a given annular element, following Burton et al. (2001), to give

$$\begin{aligned}\delta T &= \frac{1}{2}\rho W^2 nc(C_\mathrm{L}\cos\phi + C_\mathrm{D}\sin\phi)\delta r \\ &= 4\pi r\rho U^2 a_2(1-a_2)F\delta r,\end{aligned} \tag{8}$$

and

$$\begin{aligned}\delta\tau &= \frac{1}{2}\rho W^2 nc(C_\mathrm{L}\sin\phi - C_\mathrm{D}\cos\phi)r\delta r \\ &= 4\pi r^3\rho U(1-a_2)a_2'\omega F\delta r.\end{aligned} \tag{9}$$

Integrating δT and $\delta\tau$ over all blade elements gives the total axial thrust and hence rotor thrust coefficient, C_T, and the total torque, which is then multiplied by ω to give the rotor power, and hence power coefficient, C_P.

2.4 Blockage-corrected blade element momentum rotor

Blade element momentum theory provides a more advanced low-order turbine model than does actuator disc theory, but because wind turbines operate in flows which are effectively unbounded, the classical blade element momentum theory does not account for the effects of flow confinement to which turbine performance is particularly sensitive. Recently, however, Vogel et al. (2018) extended the classical theory for use with tidal turbines.

To incorporate the effects of blockage, Vogel et al. (2018) replaced the unbounded flow field with the volume-flux-constrained flow field of Garrett and Cummins (2007). The blockage-corrected blade element momentum theory has been shown to provide good agreement in thrust and power with blade-resolved simulations of tidal turbine performance. Again, only a brief description of the theory is required here; further details are provided by Vogel et al. (2018).

In unbounded flow, it is assumed that the static pressure in the near-wake of the turbine recovers in the far wake to the level of the upstream static pressure. For bounded flow, however, the acceleration of the confined bypass flow results in the development of a streamwise static pressure difference, which enables the turbine to apply a higher C_T and thereby achieve a higher maximum C_P. The blockage-corrected theory accounts for this greater pressure difference by equating the axial thrust predicted by blade element theory with the change in fluid momentum predicted by the volume-flux-constrained linear momentum theory, whilst the analysis of tangential components remains the same as in the classical unbounded theory. Closure of the equations is achieved by equating the total axial thrust with the change in momentum predicted by the volume-flux-constrained actuator disc theory.

Before performing the calculations, it is necessary to provide solidity and twist profiles for the n blades, as well as the lift and drag polars of the constituent hydrofoil. The operating condition is then defined by the blockage, B, axial velocity, U, and tip speed ratio, TSR, which represents the ratio of the tangential speed of the blade tip, ωR, to U. Initial estimates

of the axial and tangential induction factors, a_2 and a_2', and wake induction factor, a_4, are also required.

The calculation sequence begins by computing the flow angle, ϕ, attack angle, α, tip correction factor, F, and the sectional forces and torque on each blade element. As in the classical theory, δT and $\delta\tau$ are integrated over all blade elements to obtain C_T and C_P. The model then solves cubic and quartic equations, respectively, to obtain a_4 and the wake bypass velocity coefficient, b_4, which are then used to obtain a_2 and a_2'. The updated induction factors are fed back into the calculation sequence, which is solved by iteration until a relative error of $< 10^{-6}$ is achieved.

As with actuator disc theory, the key parameters are the blockage, B, basin efficiency, η, and turbine tuning. In blade element theory, however, the induction factors are replaced by variables more closely related to the operation of the rotor: the tip speed ratio, TSR, which describes the rotational speed of the turbine blades, and the blade pitch angle, $\beta = \beta_\mathrm{d} + \beta_\mathrm{a}$, which comprises the design pitch angle, β_d (relevant to both fixed-pitch and variable-pitch operation), and the adjustable blade pitch angle, β_a (for variable-pitch operation only). TSR and β may be related through a_2, a_4, and b_4, to the local resistance coefficient, k, to enable direct comparison between the actuator disc and blade element momentum theories. Though suitable for this comparison, it is worth noting that k is a less ideal performance metric for the more advanced turbine model, because it is a function of not only TSR and β but also the rotor design, and so a given value of k may be obtained in many different ways. For a given rotor, k may be increased by increasing TSR, so as to increase the rotational speed of the blades, and/or reducing β_a, so as to pitch the blades to 'stall'. Conversely, k may be reduced by decreasing TSR and/or increasing β_a, so as to pitch the blades to 'feather'.

The blockage-corrected blade element momentum theory offers a more advanced low-order turbine model, but is known to provide less accurate solutions in off-design operating conditions (that is to say, far from the design TSR and β) and highly blocked flow. To account for this limitation, B is kept relatively low and the tuning parameters are restricted to a realistic range of operating conditions: $3 \leq \mathrm{TSR} \leq 8.5$ and $-5° \leq \beta_\mathrm{a} \leq 9°$, outside of which C_T and C_P are set to zero.

2.4.1 Rotor configurations

In this study, two sets of rotors are used to analyse the performance of tidal turbines operating in moderately blocked ($B = 0.16$) and highly blocked ($B = 0.314$) flow conditions. For each blockage, two rotor configurations are considered: the variable-speed, fixed-pitch rotor, which, with fewer moving parts, is simpler, less expensive, and more reliable; and the variable-speed, variable-pitch rotor, which, though more complex, offers superior performance, particularly in off-design operating conditions. Rotors designed for moderately and highly blocked flow conditions are obtained from Cao et al. (2018) and Schluntz and Willden (2015), respectively.

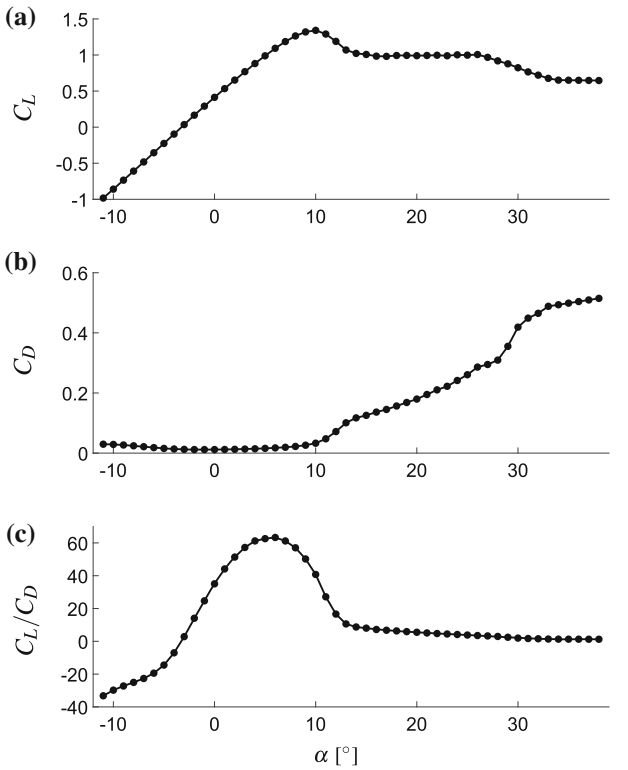

Fig. 2 Variations in: **a** lift coefficient, C_L; **b** drag coefficient, C_D, and; **c** lift-to-drag ratio, $C_\mathrm{L}/C_\mathrm{D}$; with attack angle, α, for the Risø-A1-24 hydrofoil and Reynolds number, $Re = 12 \times 10^6$. Adapted from Wimshurst and Willden (2016)

The rotors are designed using the approach proposed by McIntosh et al. (2011), in which blade element momentum methods are used to model the rotor, whilst the flow field is simulated using the three-dimensional, steady Reynolds-averaged Navier–Stokes (RANS) equations. By testing the performance of the rotor in a highly resolved numerical flume and revising its design by iteration, this approach can be used to optimise the rotor for different inflow conditions and blockage ratios (Schluntz and Willden 2015).

The rotor blades for both designs are based on the Risø-A1-24 hydrofoil, which offers a realistic ratio of maximum thickness to chord length, and a high lift-to-drag ratio over a broad range of attack angles, α. Cao et al. (2018) and Schluntz and Willden (2015) designed the rotors for an axial velocity of $U = 2\,\mathrm{m/s}$ and tip speed ratios of $TSR = 5.5$ and 5, respectively. Lift and drag polars for the analysis presented in this paper are obtained from Wimshurst and Willden (2016), and a large range of α is used to consider off-design operating conditions (Fig. 2).

It is also possible to design the rotors using only the blockage-corrected blade element momentum theory of

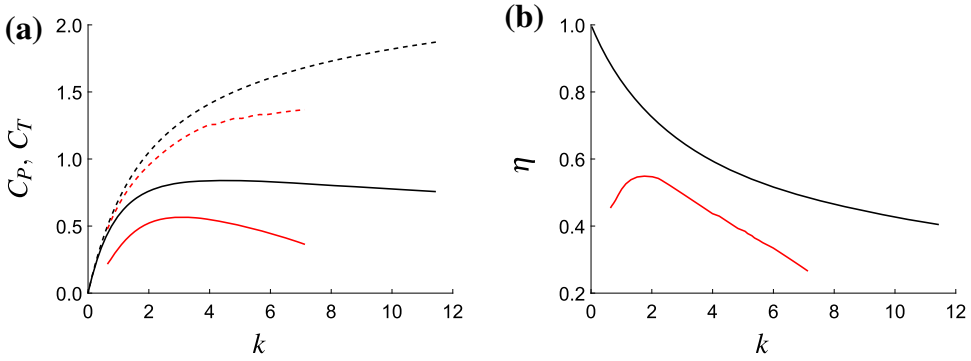

Fig. 3 Variations in: **a** power coefficient, C_P (solid lines), thrust coefficient, C_T (dashed lines), and; **b** basin efficiency, η; with local resistance coefficient, k, for an actuator disc (black lines) and fixed-pitch rotor (red lines) in moderately blocked ($B = 0.16$) flow (colour online)

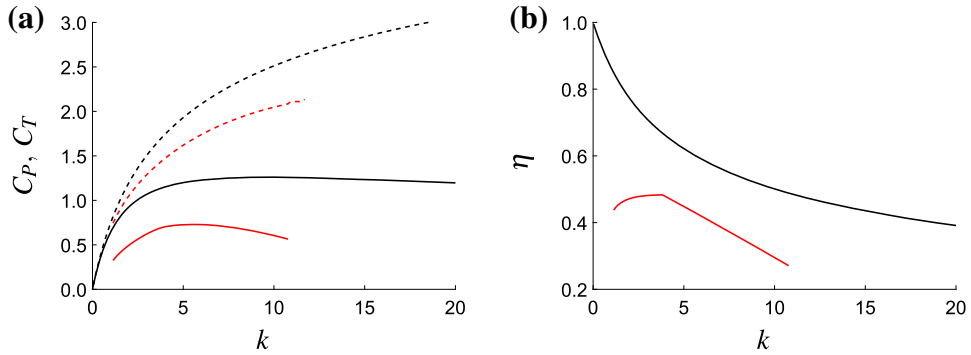

Fig. 4 Variations in: **a** power coefficient, C_P (solid lines), thrust coefficient, C_T (dashed lines), and; **b** basin efficiency, η; with local resistance coefficient, k, for an actuator disc (black lines) and fixed-pitch rotor (red lines) in highly blocked ($B = 0.314$) flow (colour online)

Vogel et al. (2018), but the physics of the constrained flow field is better captured by the three-dimensional, steady RANS equations than the idealised analytical model. Though the leading-order trends between the models should be comparable, it is worth noting that because these rotors are optimised using numerical simulations, the designs may not be strictly optimal within the analytical model, even at design operating conditions.

2.4.2 Performance curves and surfaces

The differences between the idealised actuator disc and more realistic tidal rotor are most clearly shown in Figs. 3 and 4, which compare the variations in C_P, C_T, and η with tuning, k, between variable-speed, fixed-pitch rotors and discs operating in moderately blocked ($B = 0.16$) and highly blocked ($B = 0.314$) flow conditions.

The most notable difference between the two models is that, although the variations in C_P and C_T are broadly similar, the absolute values of C_P and C_T are much lower for the rotor than for the disc (Figs. 3a, 4a). This is due to the fact that the rotor comprises a discrete number of blades which are based on a constituent hydrofoil and so, unlike the idealised disc, experience both lift and drag.

Another key difference concerns the variations in η (Figs. 3b, 4b). For the disc, there is a simple inverse relationship between k and η: as k increases, so too does C_T and thus the amount of power dissipated in local-scale wake mixing, and so η decreases. Whereas for the rotor, the relationship between k and η is more complex: as k (which, for a given fixed-pitch rotor, is represented solely by the tip speed ratio, TSR) increases, η initially increases and then decreases as the rotor emerges from a stalled flow condition (for which C_P and C_T estimates are less accurate), attains an initially large but decreasing C_P/C_T ratio, and then shuts off as the maximum permissible value of TSR is achieved. As with C_P and C_T, the absolute value of η is also lower for the more realistic rotor than for the idealised disc.

For variable-speed, variable-pitch rotors, the performance curves take the form of three-dimensional surfaces, with blade pitch angle, β_a, and tip speed ratio, TSR, on the x- and y-axes, respectively, and C_P, C_T, and η on the z-axes (Figs. 5, 6). For these rotors, the value of C_P is expected to peak at $\beta_a = 0$ and TSR $= 5.5$ (for $B = 0.16$) or 5 (for $B = 0.314$), but marginally higher values may be attained for different values of TSR for which the local thrust coefficient is no longer constant along the blade span (Schluntz and Willden 2015). C_T is shown to increase with both increasing TSR and decreasing β_a (as in pitch-to-stall operation), in contrast to η, which increases with decreasing TSR and increasing β_a (as in pitch-to-feather operation).

2.4.3 Range of operation

Blade element momentum theory is known to provide a less accurate description of turbine performance in extreme flow conditions (e.g. Moriarty and Hansen 2005). In this study, these less accurate solutions are precluded by restricting the

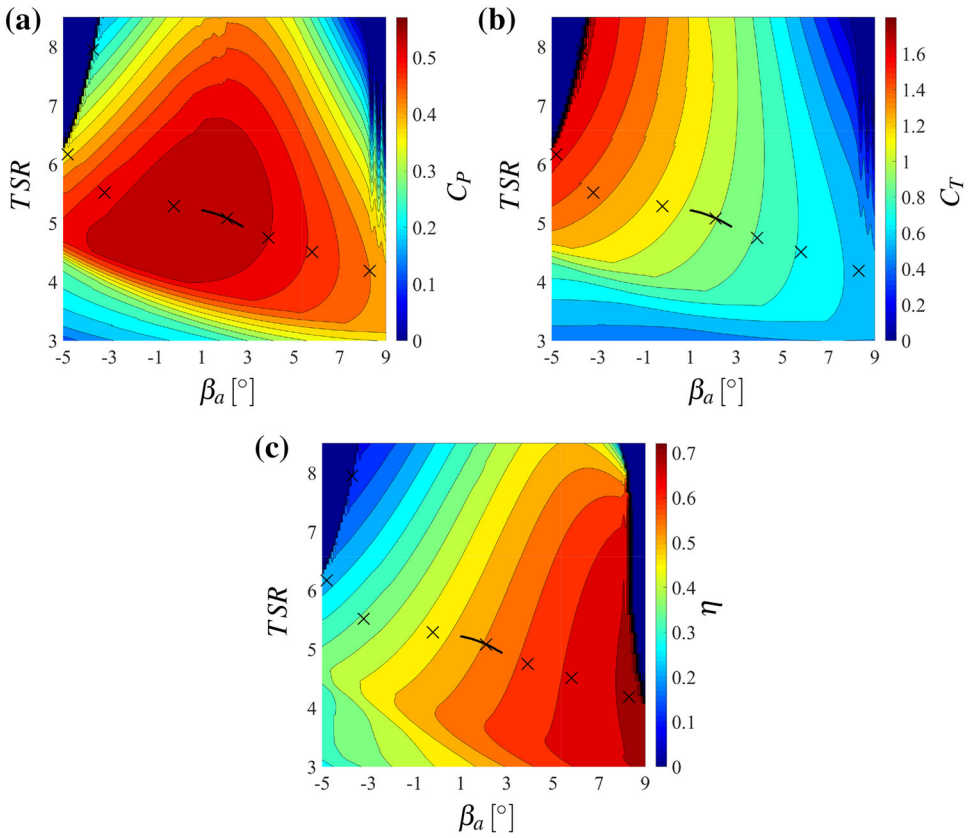

Fig. 5 Variations in: **a** power coefficient, C_P; **b** thrust coefficient, C_T, and; **c** basin efficiency, η; with tip speed ratio, TSR, and blade pitch angle, β_a, for a variable-pitch rotor in moderately blocked ($B = 0.16$) flow. Solid lines (crosses) indicate the range of operation for fixed (dynamic) turbine tuning (colour online)

range of allowable tip speed ratios ($3 \leq \text{TSR} \leq 8.5$) and blade pitch angles ($-5° \leq \beta_a \leq 9°$). Even within these ranges, however, there exist certain operating conditions for which performance results must be treated with caution.

For small TSR and large, negative β_a, for instance, results indicate that significant fractions of the blade surfaces will be operating with a very large attack angle, α. Under such an extreme stall condition, the flow will separate from the surface of the blade to such a degree that power and thrust predictions obtained from two-dimensional hydrofoil characteristics will be much less representative of actual turbine performance.

Conversely, for large TSR and large, positive β_a, the flow angle ϕ becomes sufficiently small that the calculation sequence will break down and results must instead be obtained by extrapolation. Beyond this point, however, model results become less meaningful as the rotor attains a negative induction factor and is shut down before entering its 'propeller' state.

It is worth noting that the performance maximisation strategies adopted herein will generally avoid these two extreme conditions. The solid lines and crosses in Figs. 5 and 6 indicate the maximum ranges of operation for variable-pitch rotors with fixed and dynamic tunings, respectively, and show that, for the range of flow conditions considered here, at least, maximisation of rotor power does not require the combinations of small TSR and large, negative β_a or large TSR and large, positive β_a.

Under certain conditions, however, the strategy may require the rotor to operate with large TSR and large, negative β_a. For sufficiently large k, the classical unbounded blade element momentum model attains a high induction factor ($a_2 > 0.5$) and begins to produce non-physical flow solutions as the rotor wake becomes turbulent. In this study, such solutions are avoided by shutting the rotor down when the majority (60%, say) of the primary power-producing area of the blade ($0.3 \leq r/R \leq 0.85$) exceeds a certain threshold value of a_2. Given that the wake velocity increases with blockage for a given level of thrust (Vogel et al. 2018), however, the transition to turbulence is assumed to occur at a higher induction factor ($a_2 = 0.6$, say) for both blocked flow conditions considered herein.

2.5 Turbine tuning strategies

Following Vennell (2016), three different turbine tuning strategies are used to maximise the time-averaged available power, P. For simplicity, however, this study focuses solely on maximising P, and so power-capping strategies are not considered.

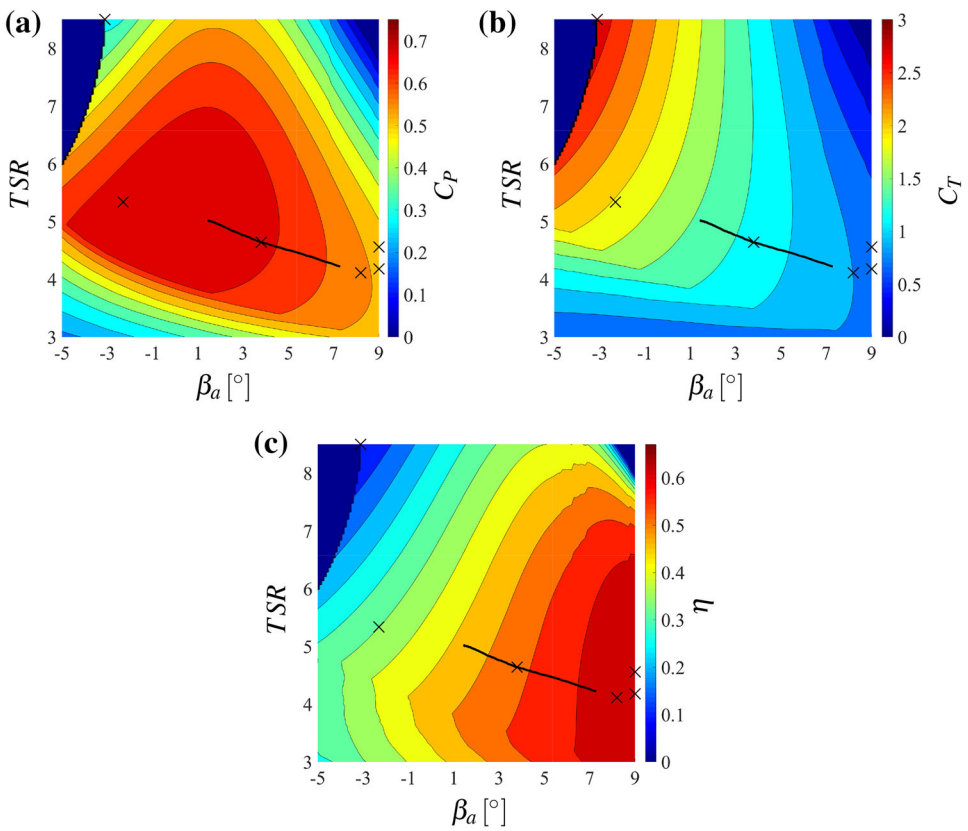

Fig. 6 Variations in: **a** power coefficient, C_P; **b** thrust coefficient, C_T, and; **c** basin efficiency, η; with tip speed ratio, TSR, and blade pitch angle, β_a, for a variable-pitch rotor in highly blocked ($B = 0.314$) flow. Solid lines (crosses) indicate the range of operation for fixed (dynamic) turbine tuning (colour online)

2.5.1 Strategy 1: impatient turbine tuning

For the first strategy, k is adjusted at each time step to ensure that C_P is maximised at each instant throughout the tidal cycle. Vennell (2016) has shown this 'impatient' tuning strategy, which is widely used in the wind energy industry, to be less beneficial for tidal turbines and so, here, the impatient strategy is used simply as a baseline for comparison.

2.5.2 Strategy 2: fixed turbine tuning

The second strategy seeks the temporally constant k which maximises P. This much simpler 'fixed' tuning strategy was first employed by Vennell (2010) and has formed the basis of a number of tidal stream power resource assessment studies (e.g. Adcock et al. 2013).

2.5.3 Strategy 3: dynamic turbine tuning

The third strategy, which seeks the temporally varying k that maximises P, was first proposed by Adcock (2012) and further explored by Vennell and Adcock (2014) and Vennell (2016). This 'dynamic' tuning strategy aims to exploit further the dynamic nature of the tide by varying the tuning in time to maximise the effects of flow acceleration.

With dynamic turbine tuning, the optimal k typically varies over the tidal half-cycle as follows. At the beginning of the half-cycle, when the velocities are low, k is assigned a value of zero to allow the flow to accelerate uninhibited. As the velocity increases over time, k is gradually increased to the maximum permissible value near the end of the half-cycle. By applying a large resistance at this point in time, the turbines are able to stop the flow sooner so that for the next half-cycle, the peak flow rate follows the peak forcing more closely, and experiences a longer period of acceleration as a result (Vennell and Adcock 2014).

Dynamic turbine tuning is most effective where the effects of turbine resistance are most significant; that is to say, for the combination of large B, large N, and small λ_0. It is worth noting, however, that the benefits of dynamic tuning depend on maximum amount of turbine resistance, which may be much lower for actual turbines than the idealised representations considered herein.

3 Results

In this section, the performance of two different idealised representations of tidal turbines are analysed and compared: the uniformly porous disc, as described by the bounded actuator disc model of Garrett and Cummins (2007), and

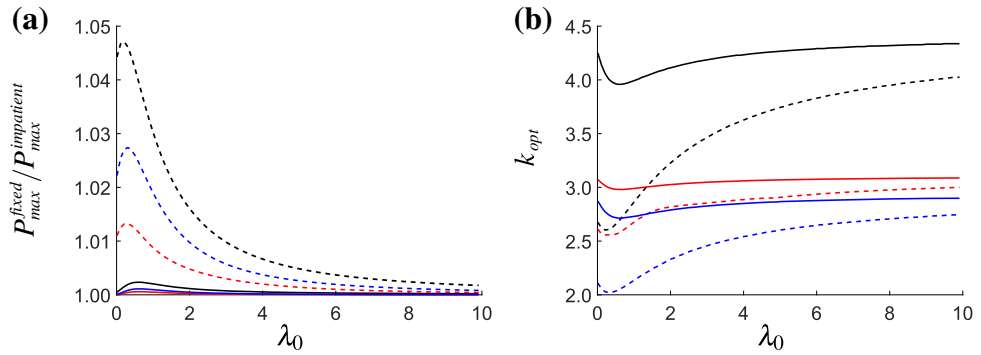

Fig. 7 Variations in: **a** normalised maximum time-averaged available power, $P_{\max}$, and; **b** optimal fixed local resistance coefficient, k_{opt}; with natural dynamic balance, λ_0, for one (solid lines) and five (dashed lines) rows of actuator discs (black), fixed-pitch rotors (red), and variable-pitch rotors (blue), in moderately blocked ($B = 0.16$) flow (colour online)

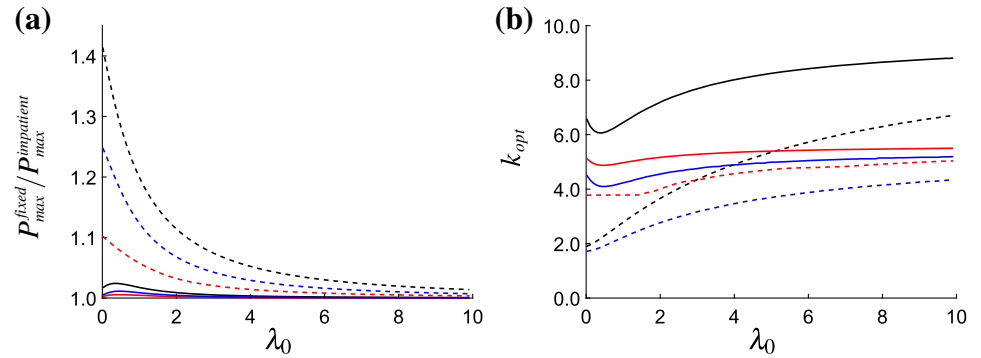

Fig. 8 Variations in: **a** normalised maximum time-averaged available power, $P_{\max}$, and; **b** optimal fixed local resistance coefficient, k_{opt}; with natural dynamic balance, λ_0, for one (solid lines) and five (dashed lines) rows of actuator discs (black), fixed-pitch rotors (red), and variable-pitch rotors (blue), in highly blocked ($B = 0.314$) flow (colour online)

the more realistic tidal rotor, as described by the blockage-corrected blade element momentum theory of Vogel et al. (2018), for which both variable-speed, fixed-pitch (FP) and variable-speed, variable-pitch (VP) designs are considered. Two primary tuning strategies are then used to maximise the time-averaged available power, P, by means of optimal fixed and dynamic tunings, k, and examine the relative importance of tuning for each turbine representation.

Though the tuning strategies focus solely on maximising P, turbine performance is discussed in terms of three key parameters: the rotor power and thrust coefficients, C_{P} and C_{T}, and the basin efficiency, η, which represents, to leading order, the ratio between C_{P} and C_{T}. The relative importance of these parameters is determined by the three variables which define the ratio of turbine drag to natural drag: the blockage, B, number of rows, N, and natural dynamic balance, λ_0, for which a broad range of values are assumed: $B = 0.16$ and 0.314, $N = 1$ and 5, and $0 \leq \lambda_0 \leq 10$.

3.1 Fixed turbine tuning

The importance of tuning is first examined by comparing the variations in $P_{\max}$ and optimal fixed k obtained using the actuator disc, FP rotor, and VP rotor with different combinations of B, N, and λ_0 (Figs. 7, 8). Power results are normalised, in this case, by those obtained using the impatient tuning strategy.

The most notable result is that, for all turbine models considered, the importance of tuning increases with increasing B, increasing N, and decreasing λ_0. This finding is consistent with existing theoretical work: Vennell (2010) has shown that when the natural drag (represented here by λ_0) is relatively low and the turbine drag (represented here by B and N) is relatively high, the effect of tuning on turbine performance is greater because the throughflow velocity, and hence available power, is more dependent on the turbine resistance.

Moreover, whilst substantial increases in power are available for large B, large N, and small λ_0, in cases where the turbine resistance is less significant (that is to say, in most practical scenarios), the fixed tuning strategy is shown to provide only slightly more power than the impatient tuning strategy.

It is also clear that, as compared to the disc, the increase in maximum available power which may be achieved by adopting a fixed tuning strategy is significantly lower for the rotors (Figs. 7a, 8a). For $B = 0.314$, $N = 5$, and $\lambda_0 = 0.01$,

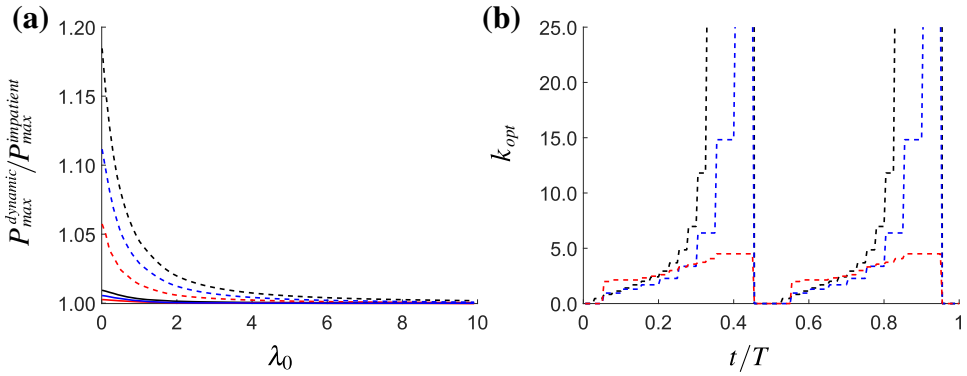

Fig. 9 Variations in: **a** normalised maximum time-averaged available power, $P_{\max}$, with natural dynamic balance, λ_0, and; **b** (near-) optimal dynamic local resistance coefficient, k_{opt}, with time, t, over the tidal cycle, T, for $\lambda_0 = 0.1$; for one (solid lines) and five (dashed lines) rows of actuator discs (black), fixed-pitch rotors (red), and variable-pitch rotors (blue), in moderately blocked ($B = 0.16$) flow (colour online)

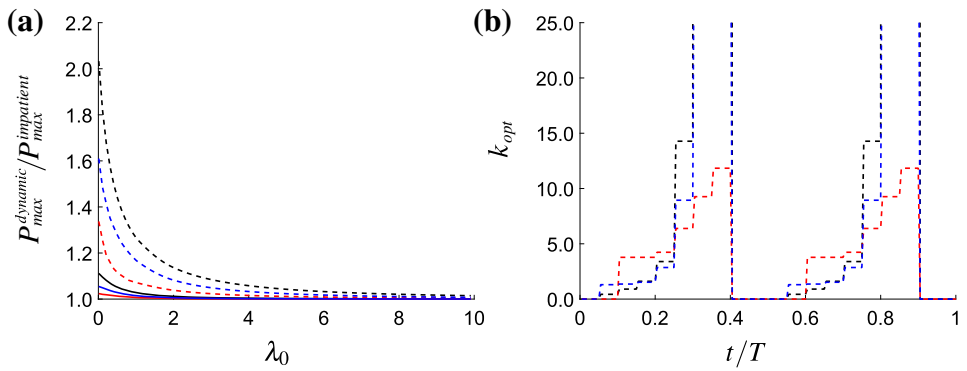

Fig. 10 Variations in: **a** normalised maximum time-averaged available power, $P_{\max}$, with natural dynamic balance, λ_0, and; **b** (near-) optimal dynamic local resistance coefficient, k_{opt}, with time, t, over the tidal cycle, T, for $\lambda_0 = 0.1$; for one (solid lines) and five (dashed lines) rows of actuator discs (black), fixed-pitch rotors (red), and variable-pitch rotors (blue), in highly blocked ($B = 0.314$) flow (colour online)

for instance, the optimal fixed tuning provides $\sim 10\%$ more power to the FP rotor than does impatient tuning, as compared to $\sim 41\%$ more power for the disc. The VP rotor performs better, providing $\sim 25\%$ more power in this case, but less significant increases for smaller B, smaller N, and larger λ_0.

To understand why the potential increase in power is lower for the rotors than the disc, it is useful to consider the variations with λ_0 of the corresponding optimal tunings, k_{opt} (Figs. 7b, 8b). Vennell (2010) explains that as λ_0 reduces and the effects of turbine resistance become more significant, the optimal fixed k for the disc generally decreases as the power becomes more dependent on the thrust coefficient, C_{T}, and basin efficiency, η, than the power coefficient, C_{P}. There is also an exception to this rule: for very small λ_0, the channel flow rate in this idealised model becomes less sensitive to the turbine resistance, and so the optimal k increases as the benefits of a higher C_{P} begin to outweigh the costs of the higher C_T and lower η.

For the rotor, however, the optimal fixed k is typically found to be lower and to undergo less variation with λ_0 than that for the disc. Tuning is shown to be less important for the more realistic rotor because the effects of turbine resistance on the throughflow velocity, and hence available power, are less significant. For large λ_0, the optimal k for the rotor is lower than for the disc because, for the more realistic turbine model, C_{P} peaks at a lower value of k (Figs. 3a, 4a). Whereas for small λ_0, the optimal k undergoes less variation with λ_0 because, for the more realistic rotor, the increase in η which accompanies a reduction in k, and thus C_{T}, is less significant (Figs. 3b, 4b).

For the FP rotor, which has no other means of controlling k, the tip speed ratio decreases significantly as the optimal k reduces, and there is a significant reduction in available power. For the VP rotor, however, pitching the blades to feather allows k to be reduced with a much smaller reduction in TSR and η. The VP rotor thus performs better than the FP rotor, particularly for small λ_0, but not quite as well as the actuator disc, for which η is much higher.

3.2 Dynamic turbine tuning

The importance of tuning is next examined by comparing the variations in P_{max} and (near-) optimal dynamic k obtained obtained for the actuator disc, FP rotor, and VP rotor. As before, different combinations of B, N, and λ_0 are considered (Figs. 9, 10), and power results are normalised by those obtained using impatient tuning.

As compared to impatient tuning, dynamic tuning is shown to provide considerably more power to the tidal rotors than does fixed tuning (Figs. 9a, 10a). Whereas, for $B = 0.314$, $N = 5$, and $\lambda_0 = 0.01$, fixed tuning provides $\sim 10\%$, $\sim 25\%$, and $\sim 41\%$ more power to the FP rotor, VP rotor, and actuator disc than impatient tuning, the corresponding increases for dynamic tuning are $\sim 34\%$, $\sim 61\%$, and $\sim 103\%$. As with fixed tuning, however, the potential increases in power are significantly lower for the more realistic rotors than for the idealised disc, and relatively small for the vast majority of cases in which the turbine resistance is less significant.

To understand why the potential increase in power is lower for the rotors than for the disc, it is useful to consider the variations with time, t, for $\lambda_0 = 0.1$, of the corresponding optimal tunings, k_{opt} (Figs. 9b, 10b). Vennell and Adcock (2014) have shown (see, for instance, their Fig. 2) that in the optimal dynamic tuning of an actuator disc, the relative importance of C_P, C_T, and η varies over the tidal cycle. As such, the half-cycle may be divided into four main phases: phase 1, in which C_T is set to zero to allow the flow to accelerate uninhibited; phase 2, in which a large η is required, as in the case of small λ_0; phase 3, in which a large C_P is required, as in the case of large λ_0, and; phase 4, in which C_T is set to its maximum value to stop the flow sooner and thus ensure an extended period of flow acceleration for the next half-cycle (Vennell and Adcock 2014).

Although there is practically no difference in optimal k between the rotor and disc during phase 1 (because the turbines are not operating), in the latter phases, and particularly near the end of the half-cycle, the differences become more apparent as the optimal k for the idealised disc approaches infinity, whilst that for the more realistic rotor remains limited.

For the VP rotor, the power output is increased by pitching the blades to feather so as to present a lower resistance during phase 1, and increasing the TSR and pitching the blades to stall so as to present a higher resistance during the latter phases. Thus, although the value of k_{opt} remains limited for the VP rotor (to $k_{opt} \approx 28$ for $B = 0.16$ and $k_{opt} \approx 45$ for $B = 0.314$), variable-pitch operation allows the rotor to more closely approximate the optimal k variations observed for the idealised disc.

3.3 Disc and rotor power comparison

Finally, the power produced by the more realistic tidal rotor is compared directly with the amount produced by the idealised actuator disc. Figures 11 and 12 show the variations with λ_0 in maximum rotor power, normalised by maximum disc power, for different combinations of B and N, and for both fixed and dynamic tunings, k.

The results show that, as expected, the idealised actuator disc consistently overestimates the amount of power available to the more realistic rotor. Across the range of variables considered, and for the specific designs chosen, the maximum available power produced by the rotors, averaged over the tidal cycle, is typically 60–70% of the amount produced by the disc. The disc is generally found to overestimate the rotor power by a greater amount when the turbine resistance is less significant (that is to say, when λ_0 is large and B and/or N are small) and the optimal k is high, and by a lesser amount when the turbine resistance is more significant (that is to say, when λ_0 is small and B and/or N are large) and the optimal k is low. As previously noted, the VP rotor is found to provide better agreement with the actuator disc model than does the FP model, because variable pitch operation allows the rotor to more closely approximate the performance of the idealised disc.

For sufficiently large λ_0, this normalised power will tend to the ratio of rotor C_P to disc C_P, the value of which will decrease with increasing B, regardless of tuning strategy. For small λ_0 and fixed tuning, the degree of agreement depends more on the ratio of rotor C_T to disc C_T, as well as the difference in η between the two models. For small λ_0 and dynamic tuning, however, the determination of the key relationship is more complicated because the relative importance of C_P, C_T, and η also changes throughout the tidal cycle importance of these variables, which changes throughout the tidal cycle.

4 Discussion and conclusions

In this paper, the works of Vennell (2010, 2016) are extended to incorporate a more realistic turbine representation, which is based on the blockage-corrected blade element momentum theory of Vogel et al. (2018). This more advanced low-order model is used to re-examine the importance of tuning for tidal turbines in channels, and to compare the actuator disc, which has been used extensively in theoretical and numerical models of tidal stream power, with a more realistic model of turbine performance.

Naturally, the results of this comparison depend on the design of the rotor. Two rotor designs were considered in this study: a moderate blockage design ($B = 0.16$) by Cao et al. (2018) and a high blockage design ($B = 0.314$) by Schluntz and Willden (2015), with the blades for both designs based

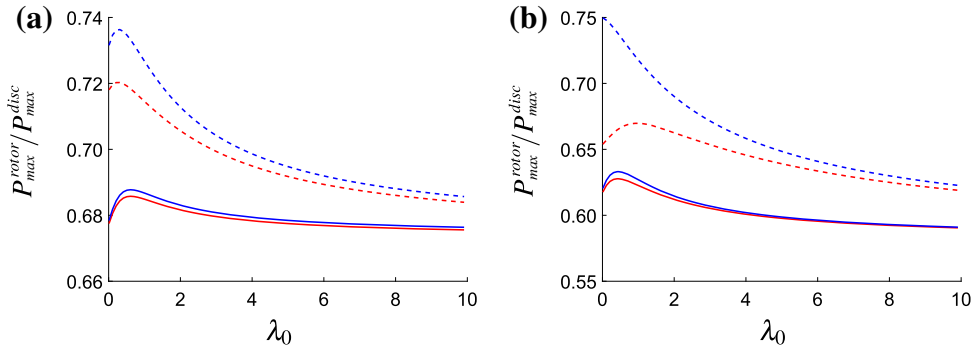

Fig. 11 Variations in normalised maximum time-averaged available power, $P_{\max}$, with natural dynamic balance, λ_0, for one (solid lines) and five (dashed lines) rows of fixed-pitch (red) and variable-pitch (blue) rotors with optimal fixed local resistance coefficient, k_{opt}, in: **a** moderately blocked ($B = 0.16$) flow, and; **b** highly blocked ($B = 0.314$) flow (colour online)

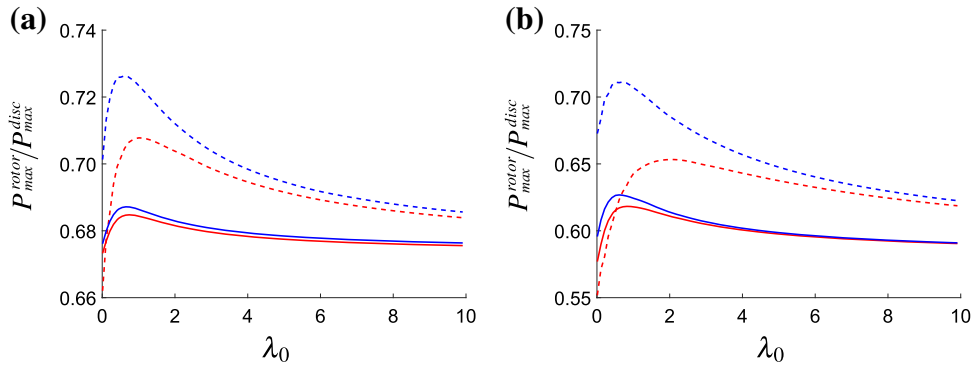

Fig. 12 Variations in normalised maximum time-averaged available power, $P_{\max}$, with natural dynamic balance, λ_0, for one (solid lines) and five (dashed lines) rows of fixed-pitch (red) and variable-pitch (blue) rotors with (near-) optimal dynamic local resistance coefficient, k_{opt}, in: **a** moderately blocked ($B = 0.16$) flow, and; **b** highly blocked ($B = 0.314$) flow (colour online)

on the Risø-A1-24 hydrofoil. The results also depend on a number of simplifying assumptions, as described in the previous sections. To minimise the influence of the inaccuracies inherent in the blade element momentum model, the blockage is kept relatively low, tuning parameters are limited to a realistic range of operating conditions, and the results from conditions in which the rotor wake becomes turbulent are excluded. Although the results of the study are necessarily specific to the rotor design and model assumptions, the overall findings should be relevant to a broad range of turbine designs and practical scenarios.

For all models considered, the effects of tuning on turbine performance are shown to be less significant when the additional drag from turbines, which is represented by the blockage, B, and number of rows, N, is small compared to the amount of natural drag, which is represented by the channel's natural dynamic balance, λ_0. This is due, simply, to the fact that tuning is less important when the throughflow velocity, and hence available power, is less dependent on the turbine resistance. Thus, whilst substantial increases in maximum available power are possible for the combination of large B, large N, and small λ_0, the benefits of a given tuning strategy will be much lower for the vast majority of cases in which the turbine resistance is less significant.

For all strategies considered, tuning is shown to be less important for the tidal rotor than for the actuator disc. For the idealised disc, large variations in the local resistance coefficient, k, may be used to produce extreme variations in thrust coefficient, C_{T}, and thus power coefficient, C_{P}, and basin efficiency, η. Depending on the flow condition, the disc may be assigned either a very large k, so as to produce a very large C_{P} (or simply a very large C_{T}, in the case of dynamic tuning), or a very small k, so as to produce a very large η. For the more realistic rotor, however, the corresponding values of C_{P}, C_{T}, and η are typically lower, and undergo less variation with k. As a result, the range of optimal k is smaller and the potential benefits of a given tuning strategy are less significant.

The results show that, as expected, the idealised actuator disc consistently overestimates the amount of power available to the more realistic blade element momentum rotor. Across the range of variables considered, the maximum available power produced by the rotors, averaged over the tidal cycle, is typically 60–70% of the amount produced by the disc. The degree of agreement will depend on the specifics of the rotor design, but the disc is generally found to overes-

timate the rotor power by a lesser amount when the turbine resistance is relatively significant (that is to say, when λ_0 is small and B and/or N are large) and by a greater amount when the turbine resistance is relatively insignificant (that is to say, in most practical scenarios). The disc is also found to overestimate the rotor power by a greater amount in the case of dynamic tuning, which, for the idealised disc, involves extreme operating conditions that cannot be matched by the more realistic rotor.

With greater flexibility in its operation, the variable-pitch rotor is able to more closely approximate the performance of the idealised disc. The adjustable blade pitch angle enables the rotor to vary the value of k whilst maintaining a near-optimal tip speed ratio, which yields benefits in terms of both power production and extraction efficiency, particularly in off-design operating conditions and cases where the turbine resistance is significant. One notable example is in the case of dynamic tuning, where, for large B, large N, and small λ_0, the variable-pitch rotor is shown to provide considerably more power than the fixed-pitch rotor.

The results also provide useful, general insights which may be used to better inform the design of tidal turbines. If a fixed tuning strategy is to be adopted, then the available power can be maximised by designing the rotor to produce either a high C_P if λ_0 is large, or a high η if λ_0 is small. If a dynamic tuning strategy is to be adopted, the task of optimal design is complicated by the fact that the rotor must provide different, and perhaps contradictory, performance characteristics throughout the tidal cycle. Given that it will be difficult to achieve the theoretically optimal temporally varying k, even with variable-pitch rotors, the necessary design compromises will limit the potential benefits of the dynamic tuning strategy. It must also be noted, however, that in most practical scenarios, the amount of turbine drag will be sufficiently small such that, for each value of λ_0, the high C_P rotor will likely produce a similar amount of power to the high η rotor, though the latter design will afford the benefits of lower structural costs and higher extraction efficiency.

Acknowledgements The authors are grateful to Bowen Cao for providing invaluable assistance in the preparation of this article.

References

Adcock TAA (2011) On the Garrett & Cummins limit. In: Proceedings of the 1st Oxford tidal energy workshop, Oxford

Adcock TAA, Draper S (2014) Power extraction from tidal channels—multiple tidal constituents, compound tides and overtides. Renew Energy 63:797–806. https://doi.org/10.1016/j.renene.2013.10.037

Adcock TAA, Draper S, Houlsby GT, Borthwick AGL, Serhadlıoğlu S (2013) The available power from tidal stream turbines in the Pentland Firth. Proc R Soc A 469(2157):20130072. https://doi.org/10.1098/rspa.2013.0072

Adcock TAA, Draper S, Nishino T (2015) Tidal power generation—a review of hydrodynamic modelling. Proc Inst Mech Eng A 229(7):755–771. https://doi.org/10.1177/0957650915570349

Betz A (1920) Das Maximum der Theoretisch Möglichen Ausnützung des Windes durch Windmotoren. Z. Gesamte Turbinenwesen 26(307–309):8

Burton T, Sharpe D, Jenkins N, Bossanyi E (2001) Wind energy handbook. Wiley, New York

Cao B, Willden RHJ, Vogel CR (2018) Effects of blockage and freestream turbulence intensity on tidal rotor design and performance. In: Progress in Renewable Energies Offshore: Proceedings of the 3rd International Conference on Renewable Energies 2018 (RENEW2018). Taylor & Francis Books Ltd, Lisbon, Portugal

Draper S, Nishino T (2014a) Centred and staggered arrangements of tidal turbines. J Fluid Mech 739:72–93. https://doi.org/10.1017/jfm.2013.593

Draper S, Nishino T (2014b) Centred and staggered arrangements of tidal turbines—Erratum. J Fluid Mech 743:636. https://doi.org/10.1017/jfm.2014.53

Draper S, Borthwick AGL, Houlsby GT (2013) Energy potential of a tidal fence deployed near a coastal headland. Phil Trans R Soc A 371(1985):20120176. https://doi.org/10.1098/rsta.2012.0176

Draper S, Nishino T, Adcock TAA, Taylor PH (2016) Performance of an ideal turbine in an inviscid shear flow. J Fluid Mech 796:86–112. https://doi.org/10.1017/jfm.2016.247

Draper S, Nishino T, Adcock TAA (2014) Turbine blockage in non-uniform flow. In: Proceedings of the 19th Australasian fluid mechanics conference, Melbourne

Eggleston DM, Stoddard FS (1987) Wind turbine engineering design. Van Nostrand Reinhold Company, New York

Garrett C, Cummins P (2005) The power potential of tidal currents in channels. Proc R Soc A 461(2060):2563–2572. https://doi.org/10.1098/rspa.2005.1494

Garrett C, Cummins P (2007) The efficiency of a turbine in a tidal channel. J Fluid Mech 588:243–251. https://doi.org/10.1017/S0022112007007781

Glauert H (1983) The elements of aerofoil and airscrew theory. Cambridge University Press, Cambridge

Gupta V, Young AM (2017) A one-dimensional model for tidal array design based on three-scale dynamics. J Fluid Mech 825:651–676. https://doi.org/10.1017/jfm.2017.399

Hau E, von Renouard H (2003) Wind turbines: fundamentals, technologies, application, economics. Springer, Berlin

Houlsby GT, Draper S, Oldfield MLG (2008) Application of linear momentum actuator disc theory to open channel flow. Tech Rep OUEL 2296/08, Department of Engineering Science, University of Oxford

Joukowsky, NE (1920) Windmill of the NEJ type. Trans Cent Inst Aero-Hydrodyn, Moscow, p 57

Kreitmair MJ, Draper S, Borthwick AGL, van den Bremer TS (2019) The effect of uncertain bottom friction on estimates of tidal current power. R Soc Open Sci 6:180941. https://doi.org/10.1098/rsos.180941

McIntosh SC, Fleming CF, Willden RHJ (2011) Embedded RANS-BEM tidal turbine design. In: Proceedings of the 9th European wave and tidal energy conference, Southampton

Moriarty PJ, Hansen AC (2005) AeroDyn theory manual. National Renewable Energy Laboratory, Golden, Colorado

Nishino T, Willden RHJ (2012) The efficiency of an array of tidal turbines partially blocking a wide channel. J Fluid Mech 708:596–606. https://doi.org/10.1017/jfm.2012.349

Schluntz J, Willden RHJ (2015) The effect of blockage on tidal turbine rotor design and performance. Renew Energy 81:432–441. https://doi.org/10.1016/j.renene.2015.02.050

Vennell R (2010) Tuning turbines in a tidal channel. J Fluid Mech 663:253–267. https://doi.org/10.1017/S0022112010003502

Vennell R (2016) An optimal tuning strategy for tidal turbines. Proc R Soc A 472(2195):20160047. https://doi.org/10.1098/rspa.2016.0047

Vennell R, Adcock TAA (2014) Energy storage inherent in large tidal turbine farms. Proc R Soc A 470(2166):20130580. https://doi.org/10.1098/rspa.2013.0580

Vennell R, Funke SW, Draper S, Stevens C, Divett T (2015) Designing large arrays of tidal turbines: a synthesis and review. Renew Sustain Energy Rev 41:454–472. https://doi.org/10.1016/j.rser.2014.08.022

Vogel CR, Houlsby GT, Willden RHJ (2016) Effect of free surface deformation on the extractable power of a finite width turbine array. Renew Energy 88:317–324. https://doi.org/10.1016/j.renene.2015.11.050

Vogel CR, Willden RHJ, Houlsby GT (2018) Blade element momentum theory for a tidal turbine. Ocean Eng 169:215–226. https://doi.org/10.1016/j.oceaneng.2018.09.018

Wimshurst A, Willden RHJ (2016) Computational analysis of blockage designed tidal turbine rotors. In: Progress in Renewable Energies Offshore: Proceedings of the 2nd International Conference on Renewable Energies 2016 (RENEW2016), Taylor & Francis Books Ltd, Lisbon, Portugal